Auger decay of neon following energetic ion bombardment*

D. L. Matthews, B. M. Johnson, J. J. Mackey, L. E. Smith, W. Hodge, and C. Fred Moore

Center for Nuclear Studies, The University of Texas at Austin, Austin, Texas 78712

(Received 27 November 1973)

A high-resolution double-focusing electrostatic electron analyzer has been used to resolve Ne Auger electrons produced by 0.15–6.0-MeV H$^+$, 1.0-MeV He$^+$, and 33-MeV 0^{5+} bombardment. Individual K-Auger satellite lines stemming from the decay of multiply ionized neon have been observed. The energies, relative intensities, and production probabilities of these satellite lines were measured as a function of the projectile Z and as a function of proton bombarding energy. Tentative identifications for all observed lines were made by comparison with calculated Auger satellite transition energies. The reliability of the Hartree-Fock calculations used was demonstrated by comparison with e^- + Ne data and by comparing calculated x-ray transition energies for multiply ionized neon to recent measurements of O + Ne x-ray lines. A rough estimate of the probability of single- and double-2s orbital vacancy production as a function of L-shell defect was obtained. With proton bombardment, the satellite-production probability Q_s was observed to decrease smoothly with increasing proton energy. The observation that Q_s for 6-MeV proton bombardment was approximately equal to that obtained with equal-velocity electrons is believed to imply that electron shakeoff is the dominant L-shell ionization mechanism for high-energy proton bombardment.

I. INTRODUCTION

To date there have been numerous measurements of x-ray and Auger-electron production in ion-atom collisions. These measurements are summarized in extensive review articles by Rudd and Macek,[1] Ogurtsov,[2] Garcia *et al.*,[3] Stolterfoht,[4] and Burch.[5]

One of the important tasks in this field is the high resolution measurement of K-Auger satellite lines produced when an atom undergoes simultaneous K- and L-shell ionization. Previously, high-resolution measurements have been restricted to photon, electron, and light-ion bombardment of gaseous targets such as Ne and Ar. The earliest high-resolution e + Ne Auger work was performed by Korber and Melborn.[6] Later measurements reporting individual satellite lines produced by ion bombardment were performed by Edwards and Rudd,[7] and by Volz and Rudd.[8] With low-energy 150–300-keV H$^+$, H$_2{}^+$, and He$^+$ bombardment, they noted a systematic increase in the satellite line intensities when increasing the projectile Z. Edwards and Rudd also reported that the relative intensities of the KL-LLL satellite lines of Ne were not the same with proton bombardment as with electron bombardment. Schneider *et al.*[9] and Stolterfoht[4] have recently extended the H$^+$ + Ne measurements to different bombarding energies. Previous measurements of proton-induced K-Auger electrons have indicated that the satellite production probability decreases with increasing projectile energy, apparently approaching the values observed in e^- + Ne measurements.

Until recently, only lower-resolution measurements[10] were available for Auger-electron production induced by moderately heavy energetic ions (30 MeV or higher). The purpose of this paper is then to report in detail the results of high resolution measurements on the Auger decay of multiply ionized neon recently performed at this laboratory.[11,12] A detailed discussion of the experimental apparatus and methods used to obtain high-resolution Auger-electron spectra is included. Tentative line identifications, which required detailed calculations of Auger-electron energies for transitions between particular terms of initial and final configurations, are also given. These calculations are tabulated and discussed for energies near observed peaks. An estimate of the production probability of 2s/2p orbital vacancies is obtained from the O^{5+} + Ne data. The accuracy of the calculations for single 2p vacancy satellite lines is demonstrated by comparison with electron bombardment data. The reliability of the calculations is further demonstrated by comparing calculated x-ray transition energies to recent measurements of the radiative decay of multiply ionized Ne.

In this paper our H$^+$ and He$^+$ data are compared with earlier measurements by Edwards and Rudd.[7] The measurement of Q_s as a function of proton bombarding energy, which has been extended to 6.0 MeV, is compared to the earlier low-resolution measurement by Schneider *et al.*[9] The peak width of the normal $KL_{2,3}L_{2,3}({}^1D_2)$ line is measured as a function of proton bombarding energy and projectile Z. Satellite-production probabilities as a function of the projectile Z are also discussed.

II. EXPERIMENTAL APPARATUS AND DETAIL

The apparatus used in these measurements has been partially described in our initial reports.[11-13] The 150–800-keV H^+ and the 1.0-MeV He^+ beams were produced at beam currents of 30–40 μA by a model JN (High Voltage Engineering Corporation) Van de Graaff accelerator. The 6.0-MeV H^+ and 33-MeV O^{5+} beams were produced by the University of Texas model EN tandem Van De Graaff accelerator at intensities of 1–2 μA. The energy and charge state of the projectiles were determined by a calibrated analyzing magnet.

With the exception of the accelerators, Fig. 1 shows schematically the main part of the experimental apparatus. The ion beams were magnetically focused to a 2-mm-diam spot before passing through a differentially pumped, all aluminum gas scattering cell having 2-mm entrance and exit apertures. After passing through the scattering cell, the ion beam was dumped into an electrostatically suppressed Faraday cup. The beam traversed a distance of 0.95 cm from the entrance to the center of the 10-cm³ volume of the scattering cell. The cell enclosure sustained the Ne target gas at a constant pressure of approximately 10 mTorr for O^{5+} +Ne measurements, and about 20 mTorr for the H^+ +Ne and He^+ +Ne experiments. The absolute pressure was measured by a thermocouple gauge mounted directly into one side of the scattering cell. The thermocouple gauge had been calibrated against a trapped McLeod gauge to ±15% of absolute pressure using Ne gas. The vacuum in the region outside the scattering cell was maintained during all measurements at 10^{-6} Torr or less by a LN_2 trapped diffusion pump. An ultraclean vacuum of at most 10^{-6} Torr was also maintained in the analyzer chamber by a turbomolecular pump.

The all aluminum analyzer chamber and the vacuum enclosure outside the scattering cell were shielded against stray magnetic fields with double layers of Permalloy. Residual magnetic field strengths were 1 mG or less within the analyzer chamber and 5 mG or less in the gas scattering cell. This slightly higher field strength existed in the scattering cell owing to the 1-cm-diam holes in the surrounding Permalloy which were necessary for entrance and exit of the ion beam.

The electron analyzer used is a Siegbahn type[14] double-focusing electron spectrometer. The mean radius of the sections of concentric spheres of this high-dispersion analyzer is 36 cm. The analyzer transmission function ($\Delta E/E$, where E is the electron energy) is 0.02% full width at half-maximum (FWHM), or 0.13–0.16 eV in the 660–840-eV electron energy range spanned in these experiments. The 10.2×0.25 mm entrance slit was mounted directly into one side of the gas scattering cell and perpendicular to the direction of the ion beam. The spectrometer was positioned to accept electrons at a fixed scattering angle of 90°. With the spectrometer acceptance angles set at 0.93° and 28.13°, the Channeltron electron multiplier was able to detect electrons electrostatically dispersed from a 0.40 mm (horizontal) ×6.25 mm (vertical) segment of the beam-target

EXPERIMENTAL SETUP

TURBOMOLECULAR PUMP

ELECTROSTATIC ANALYZER

INCIDENT BEAM

ELECTRON MULTIPLIER

FARADAY CAGE

FOCUSING MAGNET

SCATTERING CELL

HIGH-SPEED PUMPING STATION
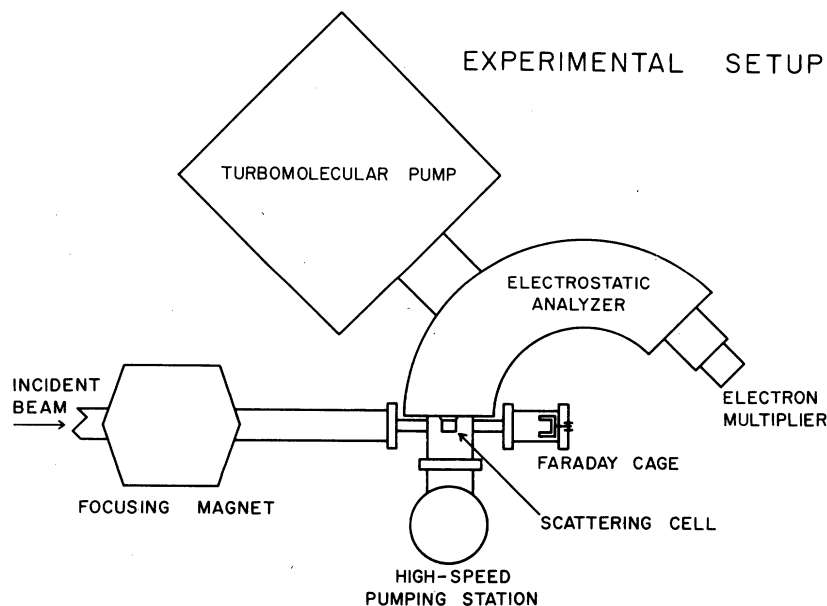
FIG. 1. Schematic representation of experimental apparatus.

interaction path.

An automatic data-collection system facilitated the production of Auger-electron spectra with good statistics and reproducibility. The number of detected electrons per fixed amount of collected ion charge and for a constant energy increment was accumulated in successive channels of computer memory. Data were stored in 4.8-mV increments of ΔV (0.011-eV change in energy of detected electrons) per channel of computer memory, where ΔV is the voltage difference between analyzer electrodes. The typical accumulation time per increment was approximately 7–8 sec. The voltages to the analyzer plates (sectors of the double-focusing analyzer) were independently controlled by the computer using high-voltage power supplies that were electrically floated atop precision 0 to ± 10 V range digital-to-analog power supplies.

Energy and efficiency calibrations of the analyzer were accomplished by substituting an electron gun for the Van de Graaff accelerator and performing elastic scattering measurements as well as comparing KLL-Auger line energies and intensities with the $e^- +$Ne data of Krause et al.[15] In the same manner we determined the analyzer constant, which proportionately relates the voltage across analyzer plates to the energy of electrons transmitted. Subsequent energies and intensities are accurate to ± 0.15 eV and 10% for strong distinct lines and ± 0.5 eV and 100% for lines which are weak and imbedded in complex spectral features. Sources of error in the relative intensities of reported lines include statistics, beam instability, pressure variation, uncertainties in background, and uncertainties in determining the analyzer transmission function as a function of energy. Sources of error in reported line energies include inaccuracies in peak fitting and fluctuations in absolute energies of lines owing to change in the work function of the scattering cell as a function of beam current and gas pressure.

An additional experimental parameter must be considered in heavy-ion–atom collisions. The charge state of the incident ion has been observed to affect the degree and amount of multiple inner-shell ionization.[16-18] Therefore, charge changing effects associated with gas target thickness and electron-capture cross section had to be carefully considered in our $O^{5+} +$Ne measurements. Single-collision scattering, implying a "thin" target,[19] was insured by noting a linear dependence of electron yield with pressure (1–50-mTorr range). To be safe, 10 mTorr was used for the $O^{5+} +$Ne measurement, which also minimized the corrections necessary for Auger-electron absorption in the scattering cell. At this pressure, the charge changing effects can be estimated by calculating[20]

$$I/I_0 = n\sigma x,$$

where I/I_0 is the fraction of the beam which undergoes a charge exchange in a gas target of thickness nx with electron-capture cross section σ. Overestimating σ at 10^{-16} cm^2/atom indicates that at most 4% of the beam underwent charge exchange before reaching the center of the scattering volume. Our target pressure is also much less than the 75–200-mTorr region used in the charge state dependence studies by Kauffman et al.[16] This lends further assurance that our target thickness has not influenced the relative production of neon charge states over what is normally attributable to O^{5+} bombardment.

III. RESULTS AND DISCUSSION

A. Calculations of Auger-electron satellite transition energies

The most important result of this experiment is the observation of individual electron lines stemming from the Auger decay of Ne^{n+} ($n = 1 - 7$).
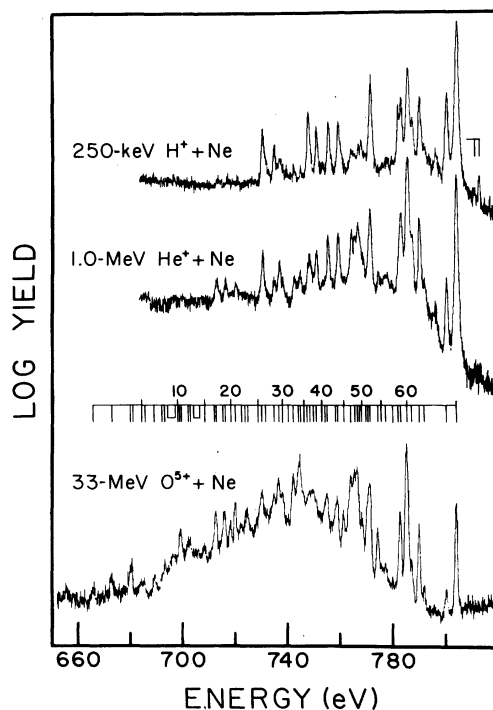
FIG. 2. Comparison of Ne K-Auger-electron spectrum produced by light- and heavy-ion impact. The "Peaks" number line above the $O^{5+} +$ Ne spectrum applies to lines observed in all spectra. Energies and intensities of all numbered lines are given in the text. This is not the complete spectrum for $O^{5+} +$ Ne collision. See Fig. 3 for more details.

Visual evidence for the increased number of satellites obtained with higher-Z projectiles can be seen in Fig. 2. The identification of the abundance of observed lines, however, has proved to be an arduous chore with relatively few unique line assignments being possible.

It is common practice to identify experimental spectral data by comparison with calculated transition energies. High-resolution Auger-electron measurements present too much detail to be compared with previously reported calculations.[21,22] Since high-resolution measurements can easily separate lines from different terms of the initial and final configurations, detailed calculations for Auger satellite lines had to be performed. Our calculations consider the Auger transitions between particular terms of the initial and final configurations instead of the previously reported[21,22] average initial and final configurations (weighted average of all multiplets).

Transition-energy calculations were performed with a Hartree-Fock computer code[23] using the adiabatic approximation. The adiabatic approximation, discussed in Ref. 3, assumes that the atom has relaxed fully to an inner-shell vacancy before an Auger transition occurs. The appropriate transition energies are given as the difference in the atom's total calculated energies for both the initial and final states. Auger transition energies (labeled by an abbreviated notation similar to that of Bhalla $et\ al.$[21]) for initial configurations $1s^l2s^m2p^n$ of neon were computed from the following expressions:

$$E_A(lmnss, {}^{2S+1}L_J - {}^{2S'+1}L'_{J'})$$
$$= E_T(1s^l2s^m2p^n, {}^{2S+1}L_J)$$
$$- E_T(1s^{l+1}2s^{m-2}2p^n, {}^{2S'+1}L'_{J'}),$$

$$E_A(lmnsp, {}^{2S+1}L_J - {}^{2S'+1}L'_{J'})$$
$$= E_T(1s^l2s^m2p^n, {}^{2S+1}L_J)$$
$$- E_T(1s^{l+1}2s^{m-1}2p^{n-1}, {}^{2S'+1}L'_{J'}),$$

$$E_A(lmnpp, {}^{2S+1}L_J - {}^{2S'+1}L'_{J'})$$
$$= E_T(1s^l2s^m2p^n, {}^{2S+1}L_J)$$
$$- E_T(1s^{l+1}2s^m2p^{n-2}, {}^{2S'+1}L'_{J'}),$$

where E_T is the total energy of a particular term $({}^{2S+1}L_J)$ of a configuration and is determined from the corresponding Hartree-Fock wave function. In addition to the Auger calculations, x-ray transition energies were computed from the expression

$$E_X(lmn, {}^{2S+1}L_J - {}^{2S'+1}L'_{J'})$$
$$= E_T(1s^l2s^m2p^n, {}^{2S+1}L_J)$$
$$- E_T(1s^{l+1}2s^m2p^{n-1}, {}^{2S'+1}L'_{J'}).$$

Following Slater,[24] E_T is defined as

$$E_T({}^{2S+1}L, nl, n'l') = E(\text{average})$$
$$+ \sum_k a_{nl,n'l',k} F^k(nl, n'l')$$
$$+ \sum_k b_{nl,n'l',k} G^k(nl, n'l'),$$

where, in this case, n is the principal quantum number and l is the orbital quantum number, E (energy) is the total energy for the average configuration, $a_{nl,n'l',k}$ and $b_{nl,n'l',k}$ are coefficients depending on the particular term being calculated in a given configuration (see Slater[24] for tabulations of a, b). F^k and G^k are electrostatic electron-electron interaction integrals. The quantities E(average), F^k, and G^k were all calculated for each defect configuration with Fischer's[23] Hartree-Fock program.

From the calculations of Auger-electron transition energies, approximately 150 satellite lines from the initial configurations $1s^12s^22p^n$ ($n = 1-6$) and over 190 satellite lines from the mixed $2s$ and $2p$ vacancy initial configurations $1s^12s^m2p^n$ ($m = 0, 1; n = 1-6$) were obtained. The Auger-electron selection rules $\Delta L = \Delta S = \Delta J = 0$ and no change in parity ($\Delta\Pi = 0$) were strictly adhered to in computing all lines (see Melhorn[25] for more details on Auger-electron selection rules). Auger satellite lines from double K-shell vacancies (hypersatellites) were also calculated, but direct experimental comparisons were not possible since these vacancies occur only a small percentage of the time.[26]

An unfortunate byproduct of detailed Auger-electron calculations is the large number of energy overlaps for calculated transitions from different defect configurations and from different types of Auger transitions ($2s2s, 2s2p, 2p2p$). This makes the unique identification of many of the experimentally observed peaks virtually impossible. Detailed calculations of Auger satellite line intensities must be performed to further clarify this picture. Auger satellite transition strengths were not calculated in this work due to numerous difficulties discussed by Schmidt.[27]

The suggested assignments for a few representative Auger transitions appear in Table I. A complete compilation of calculated and measured Auger transitions is given elsewhere.[28] All calculated satellite transitions whose energies lie within ±2 eV of a given peak are listed, unless unique identification by other means is possible. Supplementary means of identification were possible in the case of single and double $2p$ vacancy lines. Single $2p$ vacancy lines could be identified

TABLE I. Tentative assignments for observed lines.

Peak No.	Measured energy (±0.3 eV)	Calculated energy (eV)	Transition[a]	Peak No.	Measured energy (±0.3 eV)	Calculated energy (eV)	Transition[a]
1	666.1	667.6	$111pp{:}^2P^{(1)}-^1S$	52	771.3	$KL_1L_{2,3}(^1P_1)$	Normal line
2	673.3	672.5	$122ss{:}^4P-^1S$	53	771.7	771.8	$115pp{:}^2P^{(3)}-^1D$
		672.6	$102pp{:}^4P-^1S$			772.2	$115pp{:}^2P^{(1)}-^3P$
		676.4	$111pp{:}^2P^{(3)}-^1S$			772.3	$106pp{:}^2S-^1D$
16	712.5	712.0	$124ss{:}^2P-^1S$			772.4	$124pp{:}^2P-^3P$
17	713.0	713.5	$123sp{:}^3D-^4P$	54	774.5	773.5	$124sp{:}^2S-^1D$
		714.0	$123sp{:}^5S-^2D$			774.4	$125sp{:}^1P-^4P$
		714.4	$124ss{:}^4P-^3P$	55	776.3	775.6	$115pp{:}^4P-^5S$
18	715.6	716.4	$114sp{:}^5P-^4S$	56	777.6	776.1	$115pp{:}^2P^{(1)}-^3D$
19	716.2	716.8	$123sp{:}^3D-^2S$	56	777.6	776.2	$106pp{:}^2S-^3P$
		717.0	$124ss{:}^2D-^1D$	58	782.1	$KL_1L_{2,3}(^3P_{012})$	Normal line
33	744.6	744.0	$124sp{:}^4P-^3D$	59	783.1	783.6	$125pp{:}^3P-^2P$
34	745.1	744.0	$114pp{:}^5S-^4P$	60[c]	785.5	785.1	$115pp{:}^2P^{(3)}-^3D$
		744.2	$114pp{:}^3P^{(2)}-^2D$			787.3	$125pp{:}^3P-^2D$
		744.8	$114sp{:}^1P-^4S$	61	787.5	787.7	$116pp{:}^3S-^2D$
		745.5	$114pp{:}^1D-^2P$			787.9	$125pp{:}^1P-^2P$
36	747.9	$KL_1L_1(^1S_0)$	Normal line	62	790.3	789.7	$116pp{:}^1S-^2S$
40	753.6	754.6	$125sp{:}^3P-^2S$[b]			791.6	$125pp{:}^1P-^2D$[d]
41	754.4	754.6	$125sp{:}^3P-^2S$	64	800.6	$KL_{2,3}L_{2,3}(^1S_0)$	Normal line
42	755.2	755.0	$114pp{:}^1P-^2S$	65	804.2	$KL_{2,3}L_{2,3}(^1D_2)$	Normal line
		755.2	$125sp{:}^1P-^2P$	66	811.1[e]		
		755.5	$115sp{:}^2P^{(3)}-^1S$	67	813.0[e]		
51	770.7	771.5	$124pp{:}^2D-^3P$				

[a] The transition notation is defined in the text. The superscript to the right of a particular term, ^{2S+1}L, specifies parentage (e.g., $^3P^{(1)}$).

[b] Not seen in O+Ne spectrum.

[c] Unresolved doublet.

[d] Taken from Krause et al. (Ref. 14).

[e] Spectator satellites arising from 1s excitation to vacant outer orbit. See Krause et al. (Ref. 14) for discussion.

[f] Note from multiply ionized Ne. Probably a shakeup line. See Ref. 14.

by direct comparison with e^-+Ne data.[15] As reported in an earlier communication,[10] double 2p vacancy production could be identified by the presence of additional satellite lines when using a He⁺ projectile. One new means of identifying peaks, not attempted in this measurement, involves using the recent observation[16] that different bombarding particle charge states produce varying degrees of multiple ionization. In the x-ray measurements of Ref. 16, projectiles of higher charge states were observed to selectively produce higher degrees of multiple ionization in the neon target. Provided the fluorescence yield does not eliminate a substantial part of the Auger yield for high projectile charge states, then an experiment using O⁸⁺ might selectively reveal Auger satellites only from Ne⁴⁺ or higher degrees of multiple ionization.

The accuracy of the calculations for KLL normal and $KL-LLL$ satellite single 2p vacancy lines has been demonstrated[28] by comparison with the data of Krause et al.[15] The agreement for normal lines is within the accuracy of computation ($\Delta E < 1$ eV). This is as good as can be expected without abandoning pure L-S coupling and including the effects of configuration interaction (see Bhalla[29] for a discussion of configuration interaction calculations). As a further indication of the reliability of these calculations, they have been used to identify the O+Ne x-ray transitions observed by Kauffman et al.[16] A comparison[28] of calculated energies for particular x-ray transitions with observed x-ray transition energies gave close agreement (again with 1 eV) for even the two electron Ne⁸⁺ ^1P-^1S line. The accuracy of x-ray calculations using the Hartree-Fock computer code[23] for few-electron atoms has been previously verified.[30]

TABLE II. Comparison of relative intensities for various incident projectiles. D after a peak implies a normal or "diagram" transition.

Peak No.	Energy (eV)	I/I_0 (%)			Peak No.	Energy (eV)	I/I_0 (%)		
		H^+	He^+	O^{5+}			H^+	He^+	O^{5+}
1	666.1	...	...	...	35	746.3	...	...	34
2	673.3	...	...	17	36D	747.9	9.8	...	...
3	680.4	...	...	17	37	748.6	...	...	39
4	680.7	...	...	19	38	749.9	...	...	...
5	684.6	...	...	10	39	751.2	4.2	16	27
6	686.0	...	...	10	40	753.6	0.6	2.4	...
7	689.7	...	...	18	41	754.4	...	...	20
8	692.3	...	...	11	42	755.2	5.9	23	40
9	693.6	...	...	19	43	758.6	...	...	22
10	698.7	...	...	24	44	759.2	6.5	25	37
11	699.5	...	...	34	45	761.6	...	...	36
12	699.9	...	...	22	46	764.4	2.0	32	108
13	702.0	...	...	23	47	765.9	0.4	7.6	113
14	703.1	...	...	29	48	766.8	2.0	30	118
15	708.4	...	...	15	49	767.9	3.2	12	...
16	712.5	...	...	16	50	769.1	0.4	8.0	50
17	713.0	...	9.5	35	51	770.7	...	...	...
18	715.6	...	...	13	52D	771.3	26	47	...
19	716.2	...	8.2	34	53	771.7	...	...	...
20	718.4	...	...	22	54	774.5	...	...	47
21	720.4	...	7.2	41	55	776.3	...	...	15
22	722.4	...	...	15	56	777.6	...	...	19
23	724.3	...	...	16	57	780.3	...	...	11
24	725.1	...	...	22	58D	782.1	9	6.9	11
25	729.0	...	...	11	59	783.1	11	44	106
26	730.6	4.4	17	56	60	785.5	31	127	193
27	732.3	...	...	17	61	787.5	5	19	40
28	735.1	2.7	11	40	62	790.3	11	45	74
29	736.9	1.5	20	75	63	792.1	...	...	21
30	738.3	...	18	42	64D	800.6	17	19	22
31	740.5	...	...	...	65D[a]	804.2	100	100	100
32	742.5	...	6.5	73	66	811.1	0.3	...	...
33	744.6	...	...	41	67	813.0	0.8	...	...
34	745.1	0.3	9	...					

[a] Peak 65 is I_0.

B. H^+, He^+, and O^{5+} induced neon Auger-electron spectra

In Table II we compare the relative intensities for all transitions produced by H^+, He^+, and O^{5+} projectiles. The line number is keyed to the "Peaks" graph in Fig. 2. The dramatic increase in multiple inner-shell ionization for heavy-ion impact is indeed emphasized both in Table II and Fig. 2. Table III, which gives the total satellite to total Auger-electron production probabilities for various projectiles, emphasizes that the greater ionization probability of the oxygen projectile is more than velocity dependent.

A factor of 4 difference in the production of single $2p$ vacancy lines relative to normal lines between H^+ and He^+ bombardment has been previously reported.[11] This is consistent with the

Z^2 dependence in relative satellite production cross sections predicted by the direct Coulomb ionization of the K- and L-shells recently formulated by Hansteen and Mosebekk[31] in their SCA Coulomb ionization theory. For oxygen bombardment, however, the satellite production does not scale as Z^2. This discrepancy for heavy projectiles, which has also been reported in x-ray measurements, illustrates the breakdown of theoretical formulations for Coulomb ionization mechanisms in heavy-ion–atom collisions. Other details of these effects are given by Garcia et al.[3] A comparison of our H^+ +Ne spectroscopic data with similar data at different H^+ bombarding energy by Edwards and Rudd[7] and with e^- +Ne measurements is deferred to Sec. III D, where the effects of proton velocity on satellite production probability are discussed.

TABLE III. Satellite to total K-Auger-electron yields for various projectiles on neon.

Energy and projectile	Satellite Total	Ion velocity (cm/nsec)
33-MeV O^{5+}	0.94[a]	2.0
1.0-MeV He^+	0.75	0.7
0.25-MeV H^+	0.35	0.7
4.2-MeV H^+	0.23[b]	2.7
3.2-keV e^-	0.21[c]	3.2
6.0-MeV H^+	0.18	3.3

[a] Sum of intensities for resolved peaks only. The value is 0.97 if unresolved peaks are included.
[b] From Krause et al. (Ref. 14).
[c] From Stolterfoht et al. (Ref. 4).

One further comparison of the H^+ and O^{5+} bombardment data is of interest. As discussed in our first report,[12] the raw peak width (uncorrected for the transmission function of the analyzer) for the $KL_{2,3}L_{2,3}(^1D_2)$ line is 1.03 eV FWHM for O^{5+} bom-

bardment. For a velocity matched proton, the linewidth is 0.6 eV FWHM. (Linewidths for proton bombardment vary with proton velocity; see Sec. III D for more details.) Since the major contribution to these linewidths is attributed to broadening associated with target-atom recoil effects,[2] the difference in these two peak widths can be related to the momentum transferred to the target atom from the projectile. Assuming Coulombic interaction, this could then be used to determine the strength of the Coulomb field at the time of intersection. Possible usage of these peak widths as a tool for determining interaction potentials is under further scrutiny.

C. O^{5+}+Ne spectrum

The O^{5+} +Ne data merit further discussion. The observation of discrete Auger transitions above the continuous backgrounds present in heavy-ion–atom collisions is an important discovery. Unfortunately, as Table I demonstrates, the unique
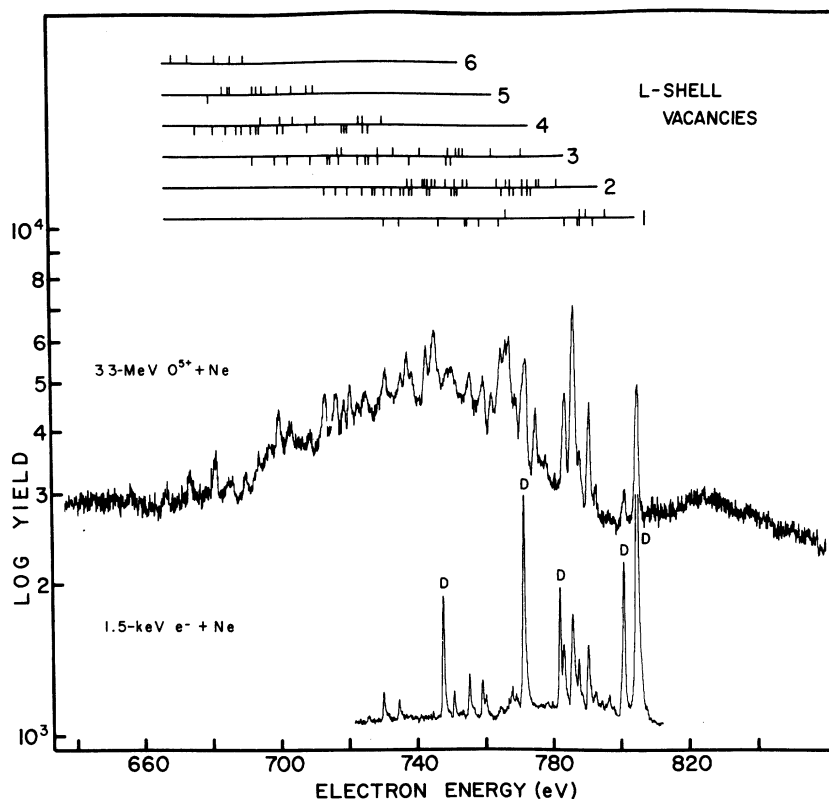
FIG. 3. Comparison of Ne K-Auger-electron spectra produced by heavy-ion and electron bombardment. The electron produced spectrum was taken with the same analyzer. In the e^- +Ne spectrum, normal or diagram Auger lines are marked D. The calculated Auger satellite transition energies are shown on the axes which label the number of L-shell vacancies. The placement of energy tick marks above a particular L-shell vacancy line denotes a transition from an initial configuration having both $2s$ and $2p$ vacancies. A tick mark below signifies that only $2p$ vacancies are present. Note the number of calculated transitions from different configurations which have nearly the same energy as an observed peak. The e^- +Ne spectrum is plotted on an arbitrary log scale. No background was subtracted from either of the displayed spectra.

identification of these satellite lines is not pres-
ently possible. Many qualitative features of the
spectra also contain spectroscopic information.
As shown with greater detail in Fig. 3, there are
two broad "humps" centered at 750 and 825 eV.
The lower-energy "hump" is tentatively attributed
to merely a superposition of weak, unresolved
lines. These lines probably result from the Auger
decay of highly ionized neon, since the "hump"
was not observed in our H^+- or He^+-induced
spectra. Calculations indicate that there could
be some contribution from Auger satellite lines
stemming from double K-shell ionization (Auger-
electron hypersatellites[21]). This same "hump" of
unresolved lines has been observed by Edwards
and Rudd[7] for low-energy Ne^+-Ne collisions. The
higher energy "hump" can be attributed either to
weak Auger hypersatellite lines or more probably
to K-LX electrons produced in the population of
$n = 3$ or higher levels by shakeup or K-shell ex-
citation. Strong evidence of K-LX lines has re-
cently been obtained by Johnson et al.[13] in high-
resolution O^{5+} + Ar L-shell Auger-electron mea-
surements.

Figure 3 also compares the K-Auger spectra
for electron and oxygen bombardment of neon.
The low- and high-energy portions of the e^- + Ne
spectrum are not included in the figure, because
no transitions were observed in these regions.
For the electron-induced spectrum, diagram lines
corresponding to $KL_1L_1(^1S_0)$, $KL_1L_{2,3}(^{1,3}P)$, and
$KL_{2,3}L_{2,3}(^1S, ^1D)$ transitions are marked D. The
unmarked strong transitions in the electron bom-
bardment spectrum are mostly due to single $2p$
vacancy satellite lines and have been discussed in
more detail by Krause et al.[15] The main purpose
for including the e^- + Ne spectrum was to demon-
strate the striking enhancement of satellite pro-
duction for oxygen as compared to electron bom-
bardment of neon. The presence of normal and
single vacancy lines in the O^{5+} + Ne spectrum is
surprising when compared with the results of neon
K x-ray measurements by Kauffman et al.[16] They
were unable to observe the normal and single L-
shell defect x-ray lines owing to the overlap in
wavelength with the hydrogenic oxygen series
limit. If present, however, these lines would ap-
parently be very weak in comparison to x-ray lines
stemming from transitions with 4, 5, and 6 L-
shell defects. The weakness of multiple L-shell
defect Auger lines combined with the observed
strength of normal and single defect Auger-elec-
tron lines (see Table II) suggests a rapid varia-
tion in fluorescence yield as a function of L-shell
defect. A quantitative measurement of the exis-
tence of such an effect, however, must await the
separation and classification of individual Auger-

electron lines for each of the L-shell defect con-
figurations. The measurement of the intensities
of the normal and single L-shell defect x-ray
lines must also be obtained.

A major motivation for doing the heavy-ion in-
duced Auger-electron measurements has been
to complement the wealth of measurements pres-
ently available for x-ray production in energetic
heavy-ion–atom collisions. One particular piece
of information which cannot conclusively be ob-
tained from high-resolution x-ray measurements
is the distribution of $2s$ to $2p$ vacancies for a
given number of L-shell defects. Bhalla and
Richard[32] discuss the sensitivity of calculated
fluorescence yields on this distribution of defects.
They conclude that the usual approximation of as-
suming a $2s$ or $2p$ defect as equivalent is not valid
when either calculating fluorescence yields or
extracting fluorescence yields from x-ray pro-
duction cross sections in low-Z elements. Auger-
electron measurements can provide the $2s/2p$
vacancy distribution since Auger satellite transi-
tion energies are sensitive to the L-shell orbital
in which a vacancy is present. Table IV presents
a rough estimate of these distributions as a func-
tion of L-shell defect. The numbers in Table IV
are given as probabilities for either pure $2p$ or
combination $2s$ and $2p$ vacancy initial configura-
tions. The tabulated values are very approximate
since they were obtained by first categorizing
the calculated satellite lines for a particular num-
ber of L-shell defects according to pure $2p$ or
mixtures of $2s$ and $2p$ defects and then counting
the number of lines from each category which
have calculated energies within ± 2 eV of an ob-
served peak. The probability of pure $2p$ or mixed
$2s, 2p$ initial vacancies is then obtained as the
ratio of the number of lines from a particular
initial vacancy category to the total number of
calculated lines with the same number of L-shell

TABLE IV. Probability of producing $2s$ vacancies for
a given number of L-shell defects. Numbers are very
approximate: They were obtained as the ratio of the
number of calculated satellite lines (whose energies lie
near that of an observed peak) from initial configura-
tions having $2s$ (or pure $2p$) defects to the total number
of lines for a particular number of L-shell defects.

Number of L-shell defects	Probability of $2s$ vacancies	Probability of pure $2p$ vacancies
6	1.0	0.0
5	0.9	0.1
4	0.6	0.4
3	0.5	0.5
2	0.4	0.6
1	0.2	0.8

defects. Despite the quantitative inaccuracy, the qualitative trend toward mixed L-subshell defects with increasing numbers of vacancies is demonstrated.

D. Dependence of satellite-production probability on proton bombarding energy

Table V compares the relative intensities of normal and satellite lines observed in 0.25-MeV H^+, 0.3-MeV H^+ (see Ref. 7), and 4.5-keV electron (see Ref. 15) collisions with neon. The larger relative intensities for satellite lines using proton rather than electron bombardment was first noted by Edwards and Rudd.[7] Further investigations of this effect have been undertaken only recently by Schneider et al.[9] Stolterfoht,[4] and our group. A description of this phenomena can be accomplished within the framework of the direct Coulomb ionization process recently discussed by Hansteen and Mosebekk.[31] In their formulation, the collision mechanism for slow protons is best described as a consecutive ionization of both the K- and L-shells via a Coulomb interaction. With this formulation, the relative ionization cross sections are energy dependent; therefore, the relative ionization probability of both K- and L-shells to pure K-shell ionization will be dependent on the projectile energy.

The description of Coulomb ionization given by Hansteen and Mosebekk[31] is well verified by experiment. A graph of Q_s, the KL (single L-shell vacancy) satellite to total Auger electron production probability as a function of proton bombarding energy is shown in Fig. 4. Our data differ quantitatively (magnitude) from that reported by Schneider et al.,[8] but this is due to the fact that we only considered single L-shell vacancy satellites (total $= Q_s$) whereas they considered all types of satellites $(\sum KL^n, n \neq 0, \text{ total} = Q_s)$. The dramatic difference

TABLE V. Comparison of relative intensities of Auger-electron transitions in neon.

Initial[a] configuration	Final[b] configuration	Energy (eV)	Relative Intensity[c] H^{+}[d]	H^{+}[e]	e^{-}[f]
$2p^6(^2S)$	$2s^02p^6(^1S_0)$	747.9	1.0	1.0	1.0
	$2s^12p^5(^1P_1)$	771.5	2.7	2.5	2.8
	$(^3P_{012})$	782.1	0.9	0.6	1.0
	$2s^22p^4(^1S_0)$	800.6	1.7	1.5	1.6
	$(^1D_2)$	804.2	10.2	7.0	10.1
$2p^5(^3P)$	$2s^02p^5(^2P)$	730.4	0.45	1.1	0.12
	$2s^12p^4(^2P)$	751.0	0.43	0.7	0.11
	(^2S)	753.6	0.06	···	0.02
	(^2D)	759.2	0.66	0.8	0.18
	(^4P)	767.9	0.33	···	0.03
	$2s^22p^3(^2P)$	783.1	1.1	1.6	0.32
	(^2D)	785.7	3.2	1.9	0.66
$2p^5(^1P)$	$2s^02p^5(^2P)$	734.9	0.3	0.3	0.09
	$2s^12p^4(^2P)$	755.6	0.6	0.5	0.23
	$2s^22p^3(^2P)$	787.6	0.5	0.9	0.24
	(^2D)	790.2	1.1	0.8	0.48

[a] Assumes $1s^12s^2$.
[b] Assumes $1s^2$.
[c] Referred to the $1s^22s^02p^6(^1S_0)$ line; $I_0 = 1.0$.
[d] $E_{H^+} = 0.25$ MeV. Relative intensities are accurate to within 10–50%, depending on the strength of the line.
[e] See ref. 6; $E_{H^+} = 0.3$ MeV.
[f] See ref. 14; $E_{e^-} = 4.5$ keV.

between 6-MeV and 150-keV H^+ induced spectra is also demonstrated in Fig. 5. Additional information is given in Table VI, where the variation in peak width for low-velocity (150-keV) protons as compared to that of high-velocity (6.0-MeV) protons is mostly due to target atom recoil broadening.[2] The amount of broadening thus represents a measure of the amount of momentum delivered to the target atom in colliding with the proton.

Electron bombardment at different energies,[33]
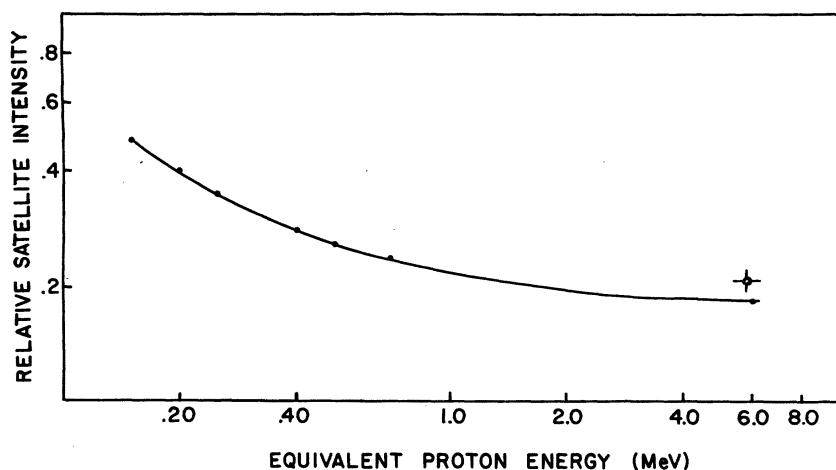
FIG. 4. Auger electron satellite production probability [yield (KL)/yield (KL) + yield (K)] is plotted versus equivalent proton energy. Error bars are 10% of the ordinate value. The starred point at 6.0 MeV is from the equivalent velocity 3.2-keV electron data reported by Krause et al,[31] but including all KL^x lines, where the x implies that all L vacancy satellite intensities were included.
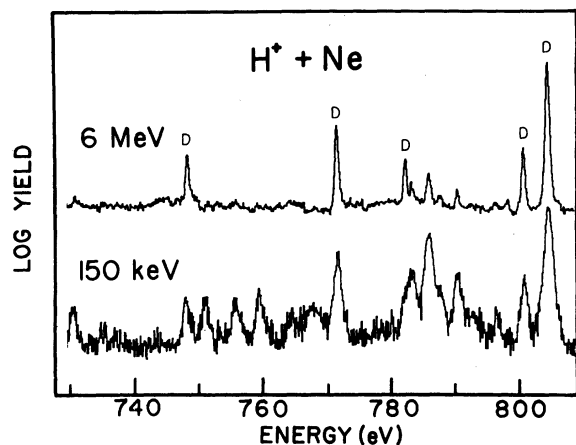
FIG. 5. Comparison of Ne K-Auger spectra produced by high- and low-energy proton bombardment. The reduction in KL satellite strength for the 6-MeV spectrum is apparent. Lines marked D are diagram lines and all others of appreciable strength are single L-vacancy (KL-LLL) satellite lines.

however, produced KL-LLL satellite lines with the same intensity relative to normal lines. Comparison of electron and photon bombardment[34] shows no differences in Q_s on the basis of excitation. These findings support electron shakeoff (sudden approximation) as the dominant L-shell mechanism for photon and electron bombardment, provided the energies of incident projectiles are sufficiently far above the ionization threshold.[33] Stolterfoht's recent measurement[4] of Q_s for 4.2-MeV H⁺ bombardment suggests that electron shakeoff can also describe high-velocity proton excitation.

IV. SUMMARY AND CONCLUSIONS

A high-resolution electrostatic electron analyzer has been successfully used to observe the Auger electrons from neon produced by light- and heavy-ion impact. The energies, relative intensities, and production probabilities of K-Auger satellite lines stemming from simultaneous single K-shell, multiple L-shell ionization of neon have been extracted as a function of projectile Z and proton bombarding energy. Auger spectra produced by electron impact are compared with those produced by "structured" oxygen ion, revealing dramatic differences. Normal KLL Auger lines were found to remain constant upon increase of projectile Z, while the satellite lines

TABLE VI. Peak widths versus proton bombardment energy in H⁺ + Ne K-Auger measurements.

Proton energy (MeV)	ΔE FWHM $KL_{2,3}L_{2,3}(^1D_2)$ line (eV)
0.15	1.06
0.20	0.81
0.40	0.73
0.50	0.67
0.60	0.64
6.0	0.51

increased in both number and intensity. The region of maximum number density of satellite lines shifts to lower energy for larger projectile Z; this is theoretically consistent with an increase in the degree of L-shell ionization.

For the O⁵⁺ + Ne collisions, more than 60 satellite lines were observed whose energies extended to 60-eV below and 40 eV above the "normal" energy region of the K-Auger spectrum. Calculated Auger-electron energies stemming from transitions having initial configurations $1s^1 2s^m 2p^n$ ($m = 0, 1, 2; n = 1-6$) were used to tentatively identify satellite lines. Since Auger transition energies are sensitive to the orbital in which L-shell ionization takes place, $2s/2p$ vacancy production as a function of L-shell defect was also obtained.

The number of satellite lines was observed to remain constant with the energy of bombarding protons. However, the ratio Q_s of the total satellite to total Auger intensity was measured to be a smoothly decreasing function of proton energy. This supports Coulomb ionization as the dominant collision mechanism in light-ion–atom scattering. Measurement of K-shell fluorescence yield as a function of L-shell defect could not be performed in these experiments. The ambiguities discovered in attempting to assign measured "peaks" to calculated Auger satellite lines could not be performed on the basis of energy comparisons alone. Detailed calculation of Auger satellite line intensities, though difficult, will be necessary to make fluorescence measurements possible.

*Work supported by the Robert A. Welch Foundation, the Air Force Office of Scientific Research, and the U. S. Atomic Energy Commission.

[1]M. E. Rudd and J. H. Macek, in *Case Studies in Atomic Collisions*, edited by E. W. McDaniel and M. R. C. McDowell (North-Holland, Amsterdam, 1972), Vol. 3, p. 47.

[2]G. N. Ogurtsov, Rev. Mod. Phys. **44**, 1 (1972).

[3]J. D. Garcia, R. J. Fortner, and T. M. Kavanagh, Rev. Mod. Phys. **45**, 111 (1973).

[4]N. Stolterfoht, in Proceedings of the VIIIth International Conference on Electronic and Atomic Collisions, Beograd, 1973, *Invited Lectures and Progress Reports*, edited by B. C. Cobic and M. V. Kurepa (Institute of Physics, Beograd, to be published).

[5]D. Burch, in Ref. 4.

[6]H. Korber and W. Melhorn, Phys. Lett. A **13**, 129 (1964); Z. Phys. **191**, 217 (1966).

[7]A. K. Edwards and M. E. Rudd, Phys. Rev. **170**, 140 (1970).

[8]D. J. Volz and M. E. Rudd, Phys. Rev. A **2**, 1395 (1970).

[9]D. Schneider, D. F. Burch, and N. Stolterfoht, *Proceedings of the VIIIth International Conference on Electronic and Atomic Collisions, Beograd, 1973, Abstract of Papers*, edited by B. C. Cobic and M. V. Kurepa (Institute of Physics, Beograd, 1973), p. 729.

[10]D. Burch, W. B. Ingalls, J. S. Risley, and R. Heffner, Phys. Rev. Lett. **29**, 1719 (1972).

[11]D. L. Matthews, B. M. Johnson, J. J. Mackey, and C. F. Moore, Phys. Lett. **45A**, 447 (1973).

[12]D. L. Matthews, B. M. Johnson, J. J. Mackey, and C. F. Moore, Phys. Rev. Lett. **31**, 1331 (1973).

[13]B. M. Johnson, D. L. Matthews, L. E. Smith, and C. F. Moore, J. Phys. B Lett. (to be published).

[14]The analyzer used is marketed commercially by McPherson Instrument Corporation, Acton, Massachusetts 01720. Design for this type of analyzer was originally discussed by K. Siegbahn *et al.*, Nova Acta Regiae Soc. Sci. Upsaliensis Ser. IV, **20** (1967).

[15]M. O. Krause, T. A. Carlson, and W. E. Moddeman, J. Phys. Paris Colloq. **C4**, 139 (1971).

[16]R. L. Kauffman, F. F. Hopkins, C. W. Woods, and P. Richard, Phys. Lett. **31**, 621 (1973).

[17]J. R. Mowat, I. A. Sellin, D. J. Pegg, R. S. Peterson, M. D. Brown, and J. R. Macdonald, Phys. Rev. Lett. **30**, 1289 (1973).

[18]J. R. Mowat, D. J. Pegg, R. S. Peterson, P. M. Griffin, and I. A. Sellin, Phys. Rev. Lett. **29**, 1577 (1972).

[19]E. N. Lassettre and S. A. Francis, J. Chem. Phys. **40**, 1208 (1964).

[20]This quantity depends on the gas density n and on the path length x traversed by the beam. Formulation for its determination is given by C. F. Barnett and H. B. Gilbody, *Methods of Experimental Physics: Atomic and Electron Physics, Atomic Interactions* (Academic, New York, 1968), Part A, Vol. 7, p. 413.

[21]C. P. Bhalla, N. O. Folland, and M. A. Hein, Phys. Rev. A **8**, 649 (1973).

[22]F. P. Larkins, J. Phys. B **4**, 14 (1971).

[23]C. F. Fischer, Comp. Phys. Commun. **1**, 151 (1969).

[24]J. C. Slater, *Quantum Theory of Atomic Structure* (McGraw-Hill, New York, 1960), Vols. I and II.

[25]W. Mehlhorn, Department of Physics Lectures, University of Nebraska, Lincoln, Nebraska (unpublished). Copies are available through Professor M. E. Rudd at that address.

[26]P. Richard, W. Hodge, and C. F. Moore, Phys. Rev. Lett. **29**, 393 (1972).

[27]V. Schmidt, in *Proceedings of the International Conference on Inner-Shell Ionization Phenomena and Future Applications, Atlanta, Georgia, 1972*, edited by R. W. Fink, J. T. Manson, I. M. Palms, and P. V. Rao (U. S. AEC, Oak Ridge, Tenn., 1973), p. 548.

[28]D. L. Matthews, B. M. Johnson and C. F. Moore (unpublished).

[29]C. P. Bhalla, Phys. Lett. **44A**, 103 (1973).

[30]D. L. Matthews, W. J. Braithwaite, H. H. Wolter, and C. F. Moore, Phys. Rev. A **8**, 1397 (1973).

[31]J. M. Hansteen and O. P. Mosebekk, Phys. Rev. Lett. **29**, 136 (1972).

[32]C. P. Bhalla and P. Richard, Phys. Lett. **45A**, 53 (1973).

[33]T. A. Carlson, W. E. Moddeman, and M. O. Krause, Phys. Rev. A **1**, 1406 (1970).

[34]M. O. Krause, F. A. Stevie, L. J. Lewis, T. A. Carlson, and W. E. Moddeman, Phys. Lett. **31A**, 81 (1970).